NORTH-HOLLAND
PHYSICS
PUBLISHING

THE EFFECT OF HELIUM CLUSTERING ON ITS TRANSPORT TO GRAIN BOUNDARIES

Nasr M. GHONIEM, Jamal N. ALHAJJI

School of Engineering and Applied Science, University of California at Los Angeles, USA

and

Dietmar KALETTA

Institut für Material-und Festkörperforschung, Kernforschungszentrum Karlsruhe, Fed. Rep. Germany

Received 28 January 1985; accepted 1 July 1985

Using a rate theory model, we develop in this investigation a solution to the problem of the rate of helium absorption at grain boundaries. In fusion reactor conditions, helium is expected to be uniformly generated inside the grains of structural materials. With the simultaniety of displacement damage production, helium atoms can be trapped in vacancies or vacancy clusters, inhibiting the migration of helium. If trapped helium is again detrapped, it will eventually find its way to grain boundaries. Helium may also be trapped on heterogeneous sites, such as precipitates. We have included both homogeneous and heterogeneous nucleation in our analysis of helium transport. It is shown that matrix clustering is an effective impediment to the transport of helium to grain boundaries only for a short irradiation time. Later, the slow leakage of helium from the matrix to grain boundaries leads to the capture of a percentage of helium produced. The role of precipitates in this mechanism is discussed. Precipitate densities below $\sim 10^{13}\ \mathrm{cm}^{-3}$ may be ineffective helium traps. The effect of displacement damage on gas resolution is discussed, and shown to have a particular significance in the determination of the average cavity density. A new mode of matrix cavity growth is suggested to result from the immobilization of a large fraction of vacancies by helium.

Reprinted from JOURNAL OF NUCLEAR MATERIALS

52

Journal of Nuclear Materials 136 (1985) 192–206
North-Holland, Amsterdam

THE EFFECT OF HELIUM CLUSTERING ON ITS TRANSPORT TO GRAIN BOUNDARIES

Nasr M. GHONIEM, Jamal N. ALHAJJI

School of Engineering and Applied Science, University of California at Los Angeles, USA

and

Dietmar KALETTA

Institut für Material-und Festkörperforschung, Kernforschungszentrum Karlsruhe, Fed. Rep. Germany

Received 28 January 1985; accepted 1 July 1985

Using a rate theory model, we develop in this investigation a solution to the problem of the rate of helium absorption at grain boundaries. In fusion reactor conditions, helium is expected to be uniformly generated inside the grains of structural materials. With the simultaniety of displacement damage production, helium atoms can be trapped in vacancies or vacancy clusters, inhibiting the migration of helium. If trapped helium is again detrapped, it will eventually find its way to grain boundaries. Helium may also be trapped on heterogeneous sites, such as precipitates. We have included both homogeneous and heterogeneous nucleation in our analysis of helium transport. It is shown that matrix clustering is an effective impediment to the transport of helium to grain boundaries only for a short irradiation time. Later, the slow leakage of helium from the matrix to grain boundaries leads to the capture of a percentage of helium produced. The role of precipitates in this mechanism is discussed. Precipitate densities below $\sim 10^{13}$ cm^{-3} may be ineffective helium traps. The effect of displacement damage on gas resolution is discussed, and shown to have a particular significance in the determination of the average cavity density. A new mode of matrix cavity growth is suggested to result from the immobilization of a large fraction of vacancies by helium.

1. Introduction

When helium atoms were introduced into a solid, either by implantation or by nuclear reactions, they tend to be insoluble. Like other noble gases, the closed electronic structure of helium results in segregation. Because of this insolubility, there is a great tendency for helium atoms to be trapped on vacancies, impurity atoms or other helium atoms [1–13].

The introduction of helium into structural materials by nuclear reactions results in a general degradation of their properties. In fast breeder reactors, as well as anticipated fusion reactors, helium generation can lead to volumetric swelling and high temperature embrittlement of structural components. It has been shown by numerous experiments [14–27], that even small amounts of helium can lead to a severe loss of ductility. Creep rupture lifetime of structural materials can therefore be drastically reduced at high temperature. Failure creep ductilities on the order of less than 1% have been reported [26].

It has also been experimentally demonstrated that the *location* of helium production is of strategic importance [27]. Steels with a small amount of boron have shown low ductility, when boron precipitates near the grain boundary. Experiments have shown that when boron atoms are uniformly distributed throughout the matrix (e.g. by thermomechanical heat treatments), the loss of ductility is not so great [27].

The problem of high temperature helium embrittlement is critical for fast breeder core and vessel structural materials. If fusion reactor first walls are operated at temperatures above 500°C for steels, helium embrittlement can also be a limiting design factor. It is therefore technologically important to address this problem. During the past two decades, there has been a significant effort to understand and solve this phenomenon (see, for example, refs. [14–27]). A great degree of understanding has been achieved. From a theoretical standpoint, the presence of helium in grain boundary cavities has been shown to result in growth instabilities that reduce the rupture lifetime [28–30]. For these treat-

0022-3115/85/$03.30

ments, however, the presence of helium inside grain boundary cavities was always assumed. For example, Trinkaus and Ullmaier [29] assumed a constant gas pressure inside growing grain boundary cavities, while Bullough, Hayns and Harries [30] assumed a simple form of gas arrival to grain boundary cavities. Even with the greater understanding of helium effects on grain boundary cavitation, there still seem to be two weak links. The first is the method of helium transport to grain boundaries. The second issue of poor understanding, is the process of grain boundary cavity nucleation.

The migration of single gas atoms to grain boundaries is complicated by the fact that there are competing matrix processes that may hinder helium transport to boundaries. Helium atoms, which predominantly migrate by an interstitital mechanism, can be trapped at precipitate interfaces, vacancies or in vacancy–helium clusters.

We have recently developed a theoretical analysis for matrix helium transport during irradiation [13]. In this paper, we develop a rate-theory based model for the study of helium migration from the matrix to the grain boundary. Helium atoms are produced in the lattice in one of the following ways:

(1) Nuclear reactions or by direct implantation. This source produces a uniform distribution of helium atoms in the matrix
(2) Displacement damage (dynamic re-solution). When helium atoms are trapped, collision cascades or direct collisions with the primary particle (neutron or ion) can displace them again into the lattice. This is an internal source of helium atoms that is also uniform over space.
(3) Localised sources. In this case, when elements such as boron are segregated near grain boundaries, a high localised source of helium is introduced. However, the burnup of boron atoms due to neutron absorption reactions leads to a transient helium source.

The first source of helium is dominant for short times, while the third is transient and relevant only for the case of neutron irradiation. The transient time scale for the third mechanism is of the order of $(\sigma_a\phi)^{-1}$, where σ is a spectral-averaged boron neutron absorption cross-section, and ϕ is the neutron flux. It will be shown later that the second mechanism is the most dominant for times longer than the time required to achieve about 1 dpa.

In the following sections we develop and apply a theory for helium clustering and transport to grain boundaries by single gas atom motion. Section 2 deals with the rate theory of helium clustering and transport. The results of calculations are presented in section 3 and conclusions follow in section 4. The symbols and their units are given in the Nomenclature.

2. Theory of helium clustering and transport to grain boundaries

In the present theoretical treatment, we will not include "localised" or "time-dependent" helium sources. In principle, the present work can be extended to allow for these inhomogeneities. Other important space or time inhomogeneities can be due to the nature of irradiation. The production of vacancies, self interstitials and helium are stochastic processes, since they are involved in collision cascades. Therefore, certain reactions between those primary species can be influenced by the time/space distribution of the production source. There is some progress in this area [31–33], however, the conclusions are not yet formulated in a way to include in a rate theory-type approach. We will therefore assume that defect reactions are homogeneous in both space and time.

Let us denote the external helium generation rate by G_{ext}^{He} (first mechanism), the internal helium generation rate by G_{int}^{He}, and the displacement damage rate by G. In this case, the total fractional helium concentration is $G_{ext}^{He}t$, where t is time. The total fractional helium displacement rate (internal source) is therefore,

$$\text{internal helium source rate} = G_{int}^{He} = G_{ext}^{He}tG. \tag{1}$$

For this source rate to exceed the external rate of helium introduction,

$$G_{ext}^{He}\tau G \geqslant G_{ext}^{He}. \tag{2}$$

Therefore, the time required to achieve this condition is of the order of

$$\tau \geqslant G^{-1}. \tag{3}$$

Of course, this is a simplified argument, and the exact value of τ will depend on the strength of the interaction between displacement damage and helium atoms [34]. However, it illustrates the point that the time required to achieve this condition is not very long, if gas re-solution rate is the same as the displacement damage rate.

In addition to single gas atom migration to grain boundaries, helium can also be transported in migrating bubbles. In this case, bubbles can move by a variety of mechanisms and transfer helium atoms with them. Once a helium atom is trapped in a vacancy, it forms a substitutional atom until other gas atoms or vacancies

react with it. If that happens, a vacancy–helium complex is said to be formed. Such a vacancy–helium complex can grow in principle by one or all of the following three processes: (1) it can accept newly created, injected or re-dissolved gas atoms; (2) it can accept vacancies either by producing nearby-Frenkel pairs in the low temperature regime ($T < 0.3T_m$, where T_m is the melting temperature in Kelvin) or by absorbing excess radiation-produced vacancies at high temperatures; and (3) it can migrate until it coalesces with other bubbles. The first two mechanisms are likely to operate in the presence of irradiation, while the last can proceed under irradiation as well as under post-irradiation conditions. Since in this case bubble migration is the rate-controlling step for bubble growth, bubble coalescence occurs only in the high temperature regime, i.e. above $0.5T_m$ [35].

The driving force for bubble migration can be either the Brownian motion in the absence of temperature or stress gradients, or sweeping by moving dislocations. In the first case bubble migration is random while in the latter cases it is directed up the gradient. Bubble motion practically stops when the bubble radius become large (~ 100 nm), or when restoring forces occur. A simple mechanism of delay is the self-pinning of bubbles by their own stress fields. This may occur when the internal gas pressure is so high as to plastically deform the surrounding matrix. Recently, gas pressures indicating solid state conditions have been measured for aluminum and nickel [36]. Important pinning centers for bubbles are the dislocations with a restoring force assumed to be constant, precipitates and grain boundaries with forcing increasing linearly with bubble radius [35].

The term "bubble" used here applies to a gas-filled cavity with a dimater above the resolution limit of the transmission electron microscope (~ 1.0 nm). Below this limit, we consider the bubble to be a "vacancy–helium cluster". Although different theoretical mechanisms exist for bubble resolution, experimental observations suggest that bubbles are highly stable defects. Possible re-solution processes are:

(1) Re-solution or shrinkage by gas-displacement events.
(2) Re-solution of small bubbles due to Ostwald ripening by vacancy or helium emission.
(3) Absorption of bubbles by others during coalescence.

Direct observations of fission gas bubble re-solution have been reported [37]. We will therefore consider dynamic re-solution to exist for helium bubbles in metals as well. Bubble growth by Ostwald ripening has been proposed [35], but experimental evidence is still missing. From both post-irradiation annealing experiments and irradiation experiments, the disappearance of small bubbles due to coalescence has been concluded. Bubble growth observations versus time growth exponent α larger than 3, when a power-law ($r \sim t^{1/\alpha}$) is applied, have been attributed to coalescence growth [35]. Theoretically, however, it could be shown that any growth exponent between 1.5 and 6 can be achieved under irradiation independent of the net flux of helium to bubbles [35]. Thus, it seems to be questionable, whether the growth mechanism represented by the α-value can be concluded from a simple power-law growth behavior.

The mode of cavity nucleation is important to discuss here. Recent stability line analyses [38,39] has shown that there are two general modes of cavity nucleation. The first mode driven by helium gas, which has been termed "spontaneous" nucleation, is dominant for high helium to dpa ratios (> 5). The second mode is what is termed stochastic nucleation by the condensation of vacancies on themselves or residual impurities. This occurs at low helium to dpa ratios. We will only consider spontaneous nucleation in the present work.

2.1. Rate equations

We will write here appropriate rate equations for the following species: (1) unoccupied vacancies; (2) self interstitial atoms; (3) interstitial helium atoms; (4) substitutional helium atoms; (5) di-interstitial helium atom clusters; (6) di-helium single vacancy clusters; (7) bubble nuclei containing 3 helium atoms; (8) large bubbles containing m helium atoms. We also develop equations for the average bubble size, the average number of helium atoms in a bubble, and the amount of helium absorbed on grain boundaries. For the case of the existence of matrix precipitates, we assume that one helium bubble is associated with each precipitate. Therefore, we include an equation describing the average precipitate bubble radius, and another equation for the average number of helium atoms in a bubble. The following are equations for the fractional concentrations of various species:

(1) Unoccupied vacancies

$$\begin{aligned} dC_v/dt = {} & fG + E^h_{gv}C_{gv} + bGC_{gv} - \alpha C_v C_i \\ & - R_{g,v}C_g C_v - R_{v,s}C^v_s C_v - R_{v,2g}C_v C_{2g} \\ & - R_{v,gv}C_v C_{gv} - R_{v,2gv}C_v C_{2gv} - R_{v,*}C_v C^*. \end{aligned} \quad (4)$$

(2) Self interstitials

$$\begin{aligned} dC_i/dt = {} & fG - \alpha C_v C_i - R_{i,gv}C_i C_{gv} - R_{i,s}C_i C^i_s \\ & - R_{i,2gv}C_i C_{2gv} - R_{i,*}C_i C^*. \end{aligned} \quad (5)$$

(3) Interstitial helium

$$\begin{aligned}\mathrm{d}C_g/\mathrm{d}t = {} & G_H + E^h_{gv}C_{gv} + bGC_{gv} + R_{i,gv}C_iC_{gv} + m_1bGC_b \\ & + bGM_{gb} + bGM_{ppt} + 2R_{i,2gv}C_iC_{2gv} \\ & + E^h_{2gv}C_{2gv} + 3bGC^* + R_{i,*}C_iC^* \\ & + 2(2bG)C_{2g} + 2bGC_{2gv} - R_{g,b}C_gC_b \\ & - R_{g,v}C_gC_v - 2R_{g,g}C_g^2 - R_{g,gv}C_gC_{gv} \\ & - R_{g,2gv}C_gC_{2gv} - R_{g,gb}C_gC_{gb} - R_{g,*}C_gC^* \\ & - R_{g,2g}C_gC_{2g} - R_{g,ppt}C_{ppt}C_g. \end{aligned} \quad (6)$$

(4) Substitutional helium

$$\begin{aligned}\mathrm{d}C_{gv}/\mathrm{d}t = {} & R_{g,v}C_gC_v + E^h_{2gv}C_{2gv} + 2bGC_{2gv} \\ & - C_{gv}\left\{E^h_{gv} + bG + R_{i,gv}C_i + R_{g,gv}\right\}. \end{aligned} \quad (7)$$

(5) A cluster of 2-helium atoms and one vacancy

$$\begin{aligned}\mathrm{d}C_{2gv}/\mathrm{d}t = {} & R_{g,gv}C_gC_{gv} + 3bGC^* + R_{v,2g}C_vC_{2g} \\ & - R_{g,2gv}C_gC_{2gv} - 2bGC_{2gv} - E^h_{2gv}C_{2gv} \\ & - R_{i,2gv}C_iC_{2gv}. \end{aligned} \quad (8)$$

(6) Di-interstitial helium clusters

$$\begin{aligned}\mathrm{d}C_{2g}/\mathrm{d}t = {} & R_{g,g}C_g^2 - R_{v,2g}C_vC_{2g} - R_{g,2g}C_gC_{2g} - 2bGC_{2g} \\ & + R_{i,*}C_iC^* - E^h_{2g}C_{2g}. \end{aligned} \quad (9)$$

(7) Bubble nucleus

$$\begin{aligned}\mathrm{d}C^*/\mathrm{d}t = {} & R_{g,2gv}C_gC_{2gv} + R_{g,2g}C_gC_{2g} - R_{g,*}C_gC^* \\ & - R_{v,*}C_vC^* - R_{i,*}C_iC^* - 3bGC^*. \end{aligned} \quad (10)$$

(8) Matrix bubble concentration

$$\mathrm{d}C_b/\mathrm{d}t = \frac{4}{m_1}R_{g,*}C_gC^* + \frac{3}{m_1}R_{v,*}C_vC^*. \quad (11)$$

(9) Average number of gas atoms in a matrix bubble

$$\mathrm{d}m_1/\mathrm{d}t = R_{g,b}C_g - bGm_1. \quad (12)$$

(10) Average matrix bubble radius

$$\begin{aligned}\mathrm{d}R/\mathrm{d}t = {} & \frac{1}{R}\Bigg(D_vC_v - D_iC_i \\ & - D_vC_v^e\left\{\exp\left[\frac{\Omega}{kT}\left(\frac{2\gamma_b}{R} - p_1\right)\right] - 1\right\}\Bigg). \end{aligned} \quad (13)$$

(11) Grain boundary gas

$$\mathrm{d}M_{gb}/\mathrm{d}t = R_{g,gb}C_g - bGM_{gb}. \quad (14)$$

(12) Average precipitate bubble radius

$$\begin{aligned}\frac{\mathrm{d}R_{pb}}{\mathrm{d}t} = {} & \left(R_{pb}^2 + r_p^2\right)^{-1/2}\Bigg(D_vC_v - D_iC_i \\ & - D_vC_v^e\left\{\exp\left[\frac{\Omega}{kT}\left(\frac{2\gamma_b}{R_{pb}} - p_2\right)\right] - 1\right\}\Bigg). \end{aligned} \quad (15)$$

(13) Total gas on precipitates

$$\mathrm{d}M_{ppt}/\mathrm{d}t = R_{g,ppt}C_{ppt}C_g - bGM_{ppt}. \quad (16)$$

While the definitions of various symbols are given in the Nomenclature section, we give here a brief description for the basis of the previous equations. The general forms of the previous reactions are: displacement damage G, thermal emission E, radiation re-solution bG (b is the re-solution parameter), and reactions between type A and type B mobile species $R_{A,B}C_AC_B$. The first 4 equations are given for the primary reacting species; namely vacancies, self interstitials, and helium atoms. The difference between the present equations for C_v and C_i and the conventional ones is that we include here clustering reactions with helium atoms in the conservation equations. Since it is assumed that gas atoms force cavity nucleation, we have included equations for 2 gas atoms – single vacancy, and for a di-interstitial helium cluster. It can be shown that di-interstitial helium clusters are unstable at high temperature due to the low binding energy [40], and that their contribution to cavity formation is limited to the low temperature regime. A cluster of 2 helium atoms and one or no vacancies is still not the critical nucleus size, since backward reaction rates can be strong. Therefore, we consider that the critical nucleus size is a cluster of 3 gas atoms and some vacancies (need not be exactly determined). This defines the early clustering part of the process. Another larger group of bubbles is then introduced with a concentration C_b. The formation of these bubbles is achieved either by a vacancy or helium atom impingement on the critical nucleus. For helium gas atom conservation, the gas–nucleus reation rate is scaled by a factor of $4/m_1$, and the vacancy–nucleus reaction rate by a factor of $3/m_1$. These are the ratios of the number of gas atoms in the reaction to the average number of gas atoms in the large size bubble group. With this, the zeroth moment of the size distribution is conserved (total number of helium atoms). Section 2.3 will clarify this concept further.

2.2. Reaction rates

We adopt here 4 basic frequencies in the clustering system. α is the frequency of self-interstitial reaction, β

is the frequency of helium gas reaction, γ is the frequency of vacancy reaction and δ is the radiation resolution frequency. These are given by:

$$\alpha = 48\nu_i \exp\left(-E_i^m/kT\right), \quad s^{-1} \tag{17}$$

$$\beta = 48\nu_g \exp\left(-E_g^m/kT\right), \quad s^{-1} \tag{18}$$

$$\gamma = 48\nu_v \exp\left(-E_v^m/kT\right), \quad s^{-1} \tag{19}$$

$$\delta = bG, \quad s^{-1} \tag{20}$$

Also, basic thermal emission probabilities are given by the Boltzmann factors:

$$e_1 = \exp\left(-E_{vh}^B/kT\right), \tag{21}$$

$$e_2 = \exp\left(-E_{v,2h}^B/kT\right), \tag{22}$$

$$e_3 = \exp\left(-E_{v,b}^B/kT\right), \tag{23}$$

$$e_4 = \exp\left(-E_v^f/kT\right), \tag{24}$$

$$e_5 = \exp\left(-E_{2g}^B/kT\right). \tag{25}$$

The binding energies E_{vh}^B, $E_{v,2h}^B$, E_{2g}^B are determined from experiments or computer lattice calculations. The vacancy–bubble binding energy $E_{v,b}^B$ is evaluated from the work done in emitting a vacancy as follows:

$$E_{v,b}^B = E_v^f + \Delta w, \tag{26}$$

$$\Delta w = -\left(\frac{2\gamma_b}{R} - P_1\right)\Omega, \tag{27}$$

where Δw is the work done by the change in surface area and in compressing the gas. The gas pressure, p_1, is determined by using the Van der Waal's equation of state for helium, i.e.

$$p_1 = m_1 kT/\left(\tfrac{4}{3}\pi R^3 - m_1 B\right). \tag{28}$$

For high gas pressures at small radii, a virial expansion is used. The following parameters are also used in our calculations:

Vacancy diffusion coefficient $= D_v = (a^2/48)\gamma$; Self-interstitial diffusion coefficient $= D_i = (a^2/48)\alpha$; Diffusion-control combinatorial factor for bubbles $= \epsilon = (4\pi/48)(R/a)$; Equivalent dispersed vacancy sink concentration $= C_s^v$; Equivalent dispersed interstitial sink concentration $= C_s^i$; Equivalent grain boundary sink concentration $= C_{GB}$. The last three parameters are given by:

$$C_s^v = \left(\frac{a^2}{48}\right)\left[Z_v\rho + 4\pi RC_b/\Omega + 4\pi R_p^e N_p\right], \tag{29}$$

$$C_s^i = \left(\frac{a^2}{48}\right)\left[Z_i\rho + 4\pi RC_b/\Omega + 4\pi R_p^e N_p\right], \tag{30}$$

$$C_{GB} = \left(\frac{a^2}{8d}\right)\left[Z\rho + 4\pi RC_b/\Omega + 4\pi R_p^e N_p\right]^{1/2}, \tag{31}$$

where

$$R_p^e = \left(r_p^2 + R_{pb}^2\right)^{1/2} \tag{32}$$

is the effective bubble–precipitate pair radius (eq. (15) and ref. [41]). Eqs. (29) and (30) are standard rate theory expressions for distributed sink strengths, and eq. (31) is discussed in section 2.4.

With the previous notations, we re-write the reaction rates for the various processes. In the following, we take the basic combinatorial number as 48, and assume that the combinatorial number with a cluster containing n particles is simply $48n$. The subject of combinatorial number calculations for small size clusters has been extensively discussed in the literature, with no conclusive results. Combinatorial numbers between 48 and 500 have been used for point defect recombination [42,43]. However, recent Monte Carlo simulations by Fastenau [44] show a monotonic increase in the combinatorial number with n, depending on the sink density and capture criteria. We therefore assumed that this dependence is $\sim 48n$ for $n = 1$, 2, and 3 only. For larger clusters, we used conventional diffusion-limited reaction rates. Table 1 lists expressions for the various elementary reaction rates. A discussion on the grain boundary loss term is given in section 2.4.

Now the previous set of rate equations can be re-written in the following form:

$$dC_v/dt = fG + (\beta e_1 + \delta)C_{gv} - \left\{\alpha C_i + \beta C_g + \gamma\left[C_s^v + C_{gv} + 2C_{2g} + 2C_{2gv} + 3C^*\right]\right\}C_v, \tag{33}$$

$$dC_i/dt = fG - \left\{C_v + C_{gv} + 2C_{2gv} + 3C^* + C_s^i\right\}\alpha C_i, \tag{34}$$

$$dC_g/dt = G_H + (\beta e_1 + \delta + \alpha C_i)C_{gv} + (\beta e_2 + 2\delta)C_{2gv} + 3(\delta + \alpha C_i)C^* + 4\delta C_{2G} + 4\alpha C_i C_{2gv} + m\delta C_b + \delta M_{gb} + \delta M_{ppt} - \left[\epsilon C_b + C_v + 4C_g + C_{gv} + 2C_{2gv} + 2C_{2g} + C_{GB} + \epsilon_{ppt}C_{ppt}\right]\beta C_g, \tag{35}$$

$$dC_{gv}/dt = \beta C_g C_v + (\beta e_2 + 2\delta)C_{2gv} - \left\{\beta e_1 + \beta C_g + \delta + \alpha C_i\right\}C_{gv}, \tag{36}$$

$$dC_{2gv}/dt = \beta C_g C_{gv} + 3\delta C^* + 2\gamma C_v C_{2g} - \left\{2\beta C_g + 2\delta + \beta e_2 + 2\alpha C_i\right\}C_{2gv}, \tag{37}$$

$$dC_{2g}/dt = 2\beta C_g^2 + 3\alpha C_i C^* - \left\{2\gamma C_v + 2\beta C_g + 2\delta\right\}C_{2g}, \tag{38}$$

$$dC^*/dt = 2(C_{2gv} + C_{2g})\beta C_g - 3(\beta C_g + \gamma C_v + \alpha C_i + \delta)C^*, \quad (39)$$

$$dC_b/dt = (12/m_1)\beta C_g C^* + (9/m_1)\gamma C_v C^*, \quad (40)$$

$$dm_1/dt = \epsilon\beta C_g - \delta m_1, \quad (41)$$

$$dR/dt = (a^2/R)\{\gamma C_v - \alpha C_i - \gamma(e_3 - e_4)\}, \quad (42)$$

$$dM_{ppt}/dt = \epsilon_{ppt}\beta C_{ppt} C_g - \delta M_{ppt}, \quad (43)$$

$$dM_{gb}/dt = \beta C_{GB} C_g - \delta M_{gb}, \quad (44)$$

$$\frac{dR_{pb}}{dt} = \frac{a^2}{(R_{pb}^2 + r_p^2)^{1/2}}\{\gamma C_v - \alpha C_i - \gamma(e_3' - e_4)\}, \quad (45)$$

where e_3' is calculated for a precipitate bubble in a similar way to e_3.

2.3. Gas conservation

For the previous system of equations to have a realistic solution, total helium gas content should be conserved. In this case, the total amount of injected gas should be accounted for in various clusters, in bubbles, on precipitates and on grain boundaries. This means that the following equation must be satisfied:

$$M_t = G_H t = C_g + C_{gv} + 2C_{2gv} + 3C^* + m_1 C_b + M_{ppt} + M_{gb}. \quad (46)$$

The time-derivative of this equation gives:

$$G_H = \frac{dC_g}{dt} + \frac{dC_{gv}}{dt} + 2\frac{dC_{2gv}}{dt} + 2\frac{dC_{2g}}{dt} + 3\frac{dC^*}{dt} + m_1\frac{dC_b}{dt} + C_b\frac{dm_1}{dt} + \frac{dM_{ppt}}{dt} + \frac{dM_{gb}}{dt}. \quad (47)$$

The right-hand side of eq. (47) is composed of time-derivatives of various cluster concentrations. Using eqs. (35) through (41), and eqs. (43) and (44), it can be easily shown that the conservation eq. (47) is strictly satisfied. We can now calculate the *fraction* of total injected gas that ends up on the grain boundaries:

$$f_{gb} = M_{gb}/G_H t. \quad (48)$$

2.4. Grain boundary helium flux

The amount of helium arriving at the grain boundary is dependent upon the matrix sink for helium. During the early stages of irradiation, matrix precipitates and bubbles are not the dominant sink and one must take

Table 1
Elementary reaction rates

	Reactions	Emissions
Interstitial	recombination = α distributed sink = $R_{i,s}C_s^i = \alpha C_s^i$ $R_{i,gv} = \alpha$ $R_{i,*} = 3\alpha$	
Vacancy	distributed sink = γC_s^v $R_{v,2g} = 2\gamma$ $R_{v,*} = 3\gamma$ $R_{v,gv} = \gamma$ $R_{v,2gv} = 2\gamma$	$D_v C_v^e \exp\left[\frac{\Omega}{kT}\left(\frac{2\gamma}{R} - p_1\right)\right] = a^2\gamma e_3$ $D_v^e C_v = a^2\gamma e_4$
Helium gas	$R_{g,v} = \beta$ $R_{g,b} = \epsilon\beta$ $R_{g,g} = 2\beta$ $R_{g,gv} = \beta$ $R_{g,2gv} = 2\beta$ $R_{g,2g} = 2\beta$ $R_{g,*} = 3\beta$ $R_{g,gb} = C_{GB}\beta$	$E_{g,v}^h = \beta e_1$ $E_{2g,v}^h = \beta e_2$ $E_{2g}^h = \beta e_5$

into account all other helium sinks (vacancies and small size clusters). The amount of helium going to grain boundaries will be small during this phase, however. Now, suppose that helium diffuses in a medium of distributed sink strength k^2. And suppose also that the grain boundary is a perfect helium sink. The diffusion equation is then given by:

$$D_g\nabla^2 C_g + G_g - k^2 D_g C_g = \partial C_g/\partial t, \tag{49}$$

where

$$k^2 = 4\pi R C_b/\Omega + 4\pi R_p^e N_p + Z\rho + \sum (\text{small cluster sinks}). \tag{50}$$

Eq. (49) may be solved analytically for cases where the helium gas diffusion coefficient (D_g), the gas generation rate (G_g) and the sink concentration k^2 are all constants and not functions of time or space. An eigenfunction solution results in a time-series representation [45]. For time-dependent variation of D_g, G_g and k^2, Matthews and Wood [46] developed a variational method for the calculation of grain boundary gas flow. For our purposes, it is sufficient to adopt the steady-state solution given by Brailsford and Bullough [47]. The following simple expression is therefore used for the "equivalent" grain boundary sink strength:

$$C_{GB} = a^2 k/8d. \tag{51}$$

2.5. *"Constrained" and "unconstrained" cavity growth modes*

Due to the fact that we have included vacancy–gas reactions in our analysis, not all of the vacancies will be readily available for cavity growth by excess vacancy absorption. Normally, when there are only two reacting species, vacancies and interstitials, the presence of a dislocation bias toward interstitials insures a larger vacancy flux to be absorbed at cavities. The growth rate of cavities is directly related to the magnitude of dislocation bias in this case. We will describe this growth behavior as an "unconstrained" cavity growth mode. A new situation is encountered when helium atoms are included in this delicate balance process. In one form or another, vacancies and interstitials eventually recombine, except for some "biased" interstitials that end up preferentially on dislocations. The cavity growth is therefore dictated by the amount of interstitials absorbed, which has an equivalent net number of vacancies in cavities. When helium gas preferentially reacts with vacancies, some vacancies are then immobilized and therefore will not be available for cavity growth. If vacancy–helium reations are significant (i.e. the number of substitutional helium atoms is a large fraction of the total vacancy population), a larger flux of self interstitials may arrive at the cavity inhibiting its growth. If this is the case, cavities can only grow by the absorption of helium atoms, and not by an excess vacancy flux. This is a very slow growth process, since helium atoms absorbed in the cavity have to produce their own Frenkel pairs due to the excessive cavity pressure. We will describe the growth behavior in this case "constrained" as opposed to the unconstrained growth mode. In the following, we derive an analytical condition for the predominance of one of these modes of growth.

Suppose now that quasi-steady state conditions have been achieved by the previous system of equations. In this case, the vacancy and interstitial equations can be described by:

$$dC_v/dt = 0 = fG - \alpha C_v C_i - \gamma C_v C_s^v - \beta C_g C_v, \tag{52}$$

$$dC_i/dt = 0 = fG - \alpha C_v C_i - \alpha C_i C_s^i. \tag{53}$$

In eqs. (52) and (53), we have combined all vacancy sinks in the C_s^v terms, and all equivalent interstitial sinks in the C_s^i term. Notice that in these equations there is one non-symmetric reaction rate, which is the reaction rate of helium gas with vacancies. Subtracting eq. (52) from (53), and rearranging, it can be easily shown that:

$$\frac{\gamma C_v}{\alpha C_i} = \left(C_s^i/C_s^v\right) \Big/ \left(1 + \frac{\beta C_g}{\gamma C_s^v}\right). \tag{54}$$

For "unconstrained" cavity growth (eq. (42)), $\gamma c_v/\alpha C_i$ must be greater than unity. Since $\langle Z_i \rangle = C_s^i/C_s^v$, where $\langle Z_i \rangle$ is the average system bias, then the "unconstrained" growth condition is expressed as:

$$\langle Z_i \rangle \geqslant \left(1 + \frac{\beta C_g}{\gamma C_s^v}\right). \tag{55}$$

If $\langle Z_i \rangle$ is expressed as:

$$\langle Z_i \rangle = 1 + \Delta Z_i \tag{56}$$

then, the "unconstrained" growth condition is

$$\langle \Delta Z_i \rangle \geqslant \beta C_g/\gamma C_s^v. \tag{57}$$

Cavity growth can therefore be "constrained" until this condition is satisfied. In other words, the conversion condition from "constrained" to "unconstrained" growth is achieved when:

(vacancy–sink reaction rate)

$$\geqslant \langle \Delta Z_i \rangle \times (\text{vacancy–helium reaction rate}). \tag{58}$$

Eq. (58) is the necessary condition for the conversion process.

3. Results of calculations

3.1. Influence of clustering on single gas atom transport to grain boundaries

During the early stages of irradiation, helium is generated as an interstitial atom, but is soon trapped when vacancies become available. The concentration of untrapped helium is never very high. This trapping eventually leads to the formation of bubbles from substitutional helium. We first present the results of calculations for ion-irradiation conditions. This is intended to simulate a study conducted by Argonne using dual-ion beam irradiation at a nominal temperature of 625°C on type 316 stainless steel [48]. The displacement damage rate is 3×10^{-3} dpa/s, and the helium/dpa ratio is 5. While the re-solution parameter (b) has been set = 1, and the dislocation bias factor to $\langle Z_i\rangle = 1.2$; the remainder of material parameters are the standard values for 316 stainless steel, and are given in table 2. The sensitivity of the calculations to input parameters is discussed later in this section.

We will discuss the influence of matrix clustering on the transport of helium atoms to grain boundaries. Figure 1 shows the concentrations of single vacancies (C_v), self interstitials (C_i), interstitial helium (C_g), sub-

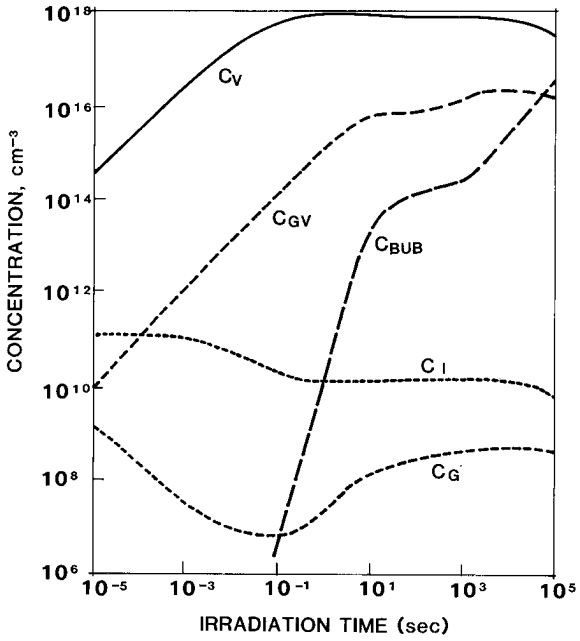

Fig. 1. The evolution of clusters and bubble concentrations as a function of irradiation time. Irradiation condition is dual ion beam with a He (appm) to dpa ratio of 5 and a damage rate of 3×10^{-3} dpa/s at 625°C.

Table 2
Standard material parameters for 316 stainless steel

Notation	Parameter	Value	Units	Ref.
a	lattice parameter	3.63	Å	[1]
k	Boltzmann's constant	8.617×10^{-5}	eV/K	
ρ	dislocation density	3×10^{10}	cm/cm^2	
d	grain diameter	3×10^{-3}	cm	[2]
E_i^m	migration energy of single interstitials	0.2	eV	[3]
E_g^m	migration energy of interstitial He	0.2	eV	
E_v^m	migration energy of single vacancy	1.4	eV	[3]
E_{vh}^B	detrapping energy of a substitutional He	2.4	eV	[39]
E_{v2h}^B	detrapping energy of a sub-He–He	3.5	eV	[39]
E_{2g}^B	detrapping energy of di-interstitial He	0.79	eV	[4]
E_v^F	formation energy of a vacancy	1.6	eV	[3]
E_i^F	formation energy of an interstitial	4.08	eV	[3]
γ_b	surface energy	6.24×10^{14}	eV/cm^2	[3]
ν_i	interstitial vibration frequency	5×10^{13}	s^{-1}	[5]
ν_g	helium vibration frequency	5×10^{13}	s^{-1}	
ν_v	vacancy vibration frequency	5×10^{12}	s^{-1}	[6]
r_p	precipitate radius	10^{-6}	cm	
N_p	precipitate number density	10^{10}	cm^{-3}	
B	Van der Waals' constant	1.75×10^{-23}		[6]
b	re-solution parameter	1		
Z_i	bias factor of interstitials	1.2		
Ω	atomic volume	1.198×10^{-23}	cm^3	[8]

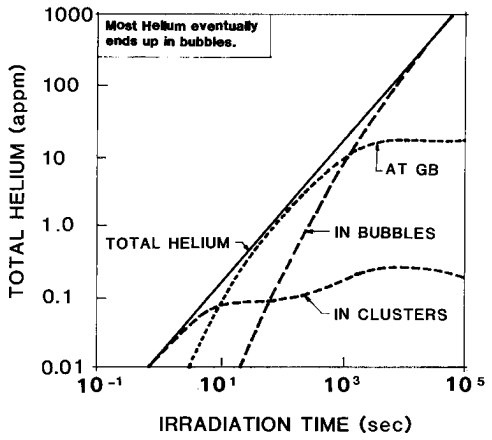

Fig. 2. Helium distribution between the different traps in the material. The irradiation condition is a He (appm)/dpa equal to 5 at 3×10^{-3} dpa/s at 625°C.

stitutional helium (C_{gv}), as well as bubbles (C_B^-). It is shown that the time structure of C_v and C_i is little affected by the presence of helium. However, the absolute magnitude of the vacancy concentration in this case is less than the corresponding case without the interaction with helium gas. After a short period of irradiation time ($t \geq 0.1$ s), more helium is produced by displacement reactions leading to a second peak in the interstitial helium concentration around 10 s, as can be seen in fig. 1. The system comes to near dynamic equilibrium in about 1000 (few dpa's). Fig. 2 shows the distribution of helium in clusters, bubbles and grain boundaries as a function of time. By definition, vacancy–helium clusters are those containing 3 helium atoms or less, while bubbles contain more than 3 helium atoms. Since the helium injection rate is constant, the total amount of helium is linear in time. During early irradiation times (< 0.01 dpa), most of injected helium resides in small helium–vacancy clusters. These are converted to bubbles at a higher dose, as shown in fig. 2. The largest proportion of helium ends up in matrix bubbles at doses greater than about 10 dpa. It is observed that during the early stages of irradiation, helium is contained in small clusters. Later, a large proportion goes to grain boundaries. However, the matrix bubble concentration becomes significant, when the fraction of helium at grain boundaries is only a few percent of total injected helium.

3.2. Comparison with experiments

Figs. 3 and 4 demonstrate the sensitivity of cavity evolution parameters to variations in the re-solution

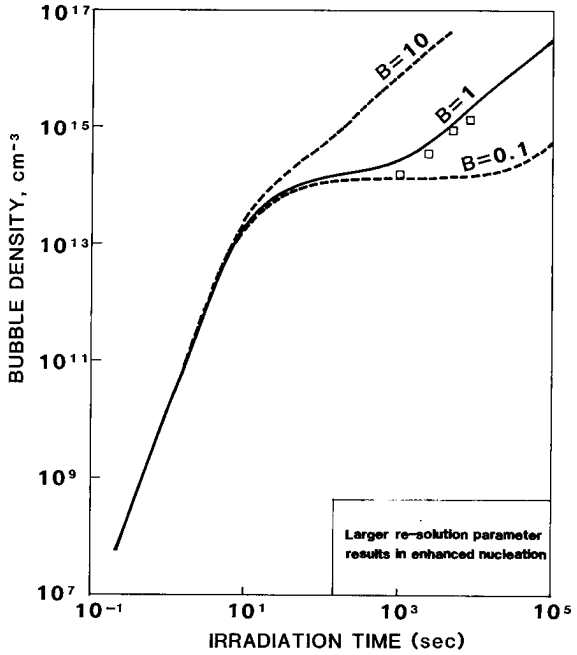

Fig. 3. The effect of re-solution parameter on the bubble concentration for dual ion beam irradiation at 625°C. The He (appm)/dpa is 5 and the damage rate is 3×10^{-3} dpa/s. (Data from ref. [48].)

rate. In fig. 3, a higher re-solution rate is shown to result in continuous cavity nucleation without saturation of the total number density. Low re-solution parameters (below 0.1) lead to saturation of the cavity number density after a short transient time. On the other hand, higher re-solution parameters result in continuous cavity nucleation. The exact value of the re-solution parameter is actually a function of the PKA energy and the cavity radius [49]. This refinement is not included in the present analysis. The effects of helium re-solution on the average matrix bubble radius is shown in fig. 4. A larger re-solution parameter leads to a higher concentration of substitutional helium, and hence to "constrained" cavity growth.

The influence of the bias factor Z_i on the microstructural parameters is demonstrated in fig. 5. The reasonable variation in Z_i shows that the model results come in agreement with experiments. The point to note in fig. 5 is the fast build-up of total cavity density. Cavity nucleation is shown to be a fast physical process. However, trailing nucleation may still persist beyond this fast phase, as illustrated in fig. 6. The nucleation current, J, is shown as a function of irradiation time for extreme parametric conditions. It is interesting to note that nucleation during the early parts of irradiation

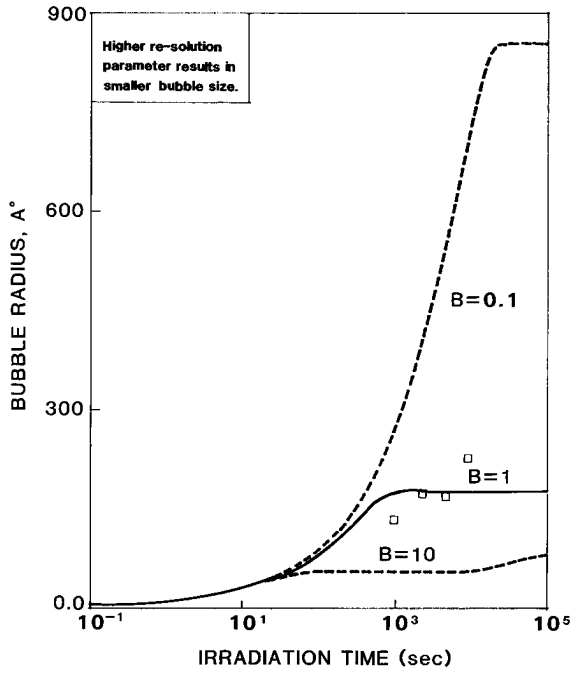

Fig. 4. The effect of the re-solution parameter on bubble growth. Irradiation condition is He (appm)/dpa is 5 at 625°C and a damage rate of 3×10^{-3} dpa/s. (Data from ref. [48].)

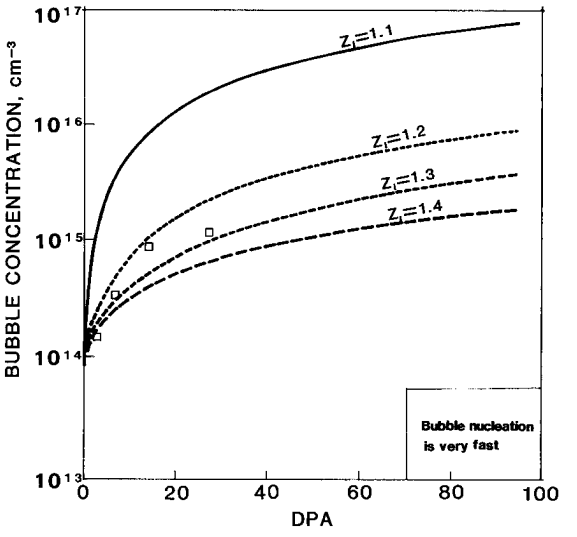

Fig. 5. The number density of bubbles is strongly affected by the interstitial bias factor Z_i. The irradiation condition is 1.5×10^{-2} appm/s and a He (appm)/dpa of 5 at 625°C. (Data from ref. [48].)

(below ~0.01 dpa) is totally insensitive to parametric variations, and is primarily dependent upon helium and dpa generation rates. Generated helium is immediately trapped in free vacancies, or by small vacancy–helium clusters. This behavior is similar to the concept of a "nucleation pulse" as described by Trinkaus [40]. Trailing nucleation may still proceed at a slower rate, dictated by irradiation conditions, for a long time. Cavity number density may therefore increase by a "crucial" few order of magnitude over the period of irradiation. We will therefore emphasize this mechanism as a "dynamic nucleation" mechanism for cavity formation. Such dynamic nucleation can be continuous throughout irradiation, if the re-solution rate is high, as demonstrated in fig. 6.

A comparison of calculations with HFIR data [50] is shown in figs. 7 and 8. The high cavity densities in HFIR experiments may be an indication of the dominance of dynamic re-solution, as well as "constrained" growth as described earlier. A comparison of this data with EBR-II data shows that cavity densities are orders of magnitude higher due to the profound influence of helium on nucleation.

3.3. Effects of pre-existing matrix precipitates and grain size on grain boundary helium gas

One practical idea to prevent grain boundary cavity nucleation, and hence mitigate helium embrittlement, is to trap the helium on matrix precipitates (see, for example, ref. [26].) This idea has been implemented in the development of titanium modified stainless steels, that

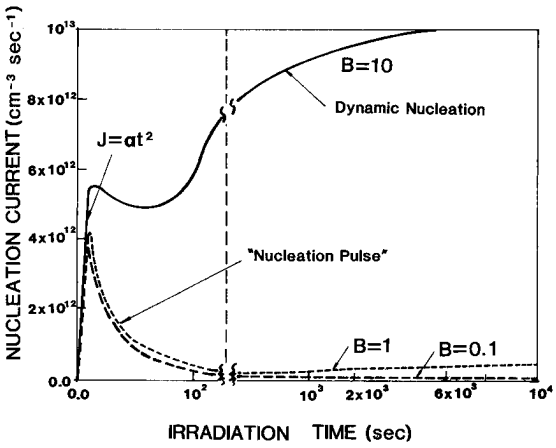

Fig. 6. The nucleation behavior of bubbles under irradiation for various values of the re-solution parameter.

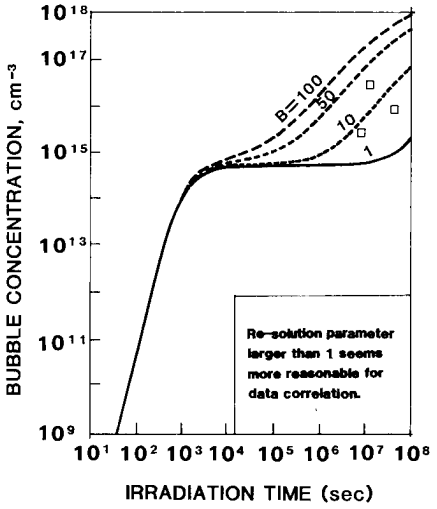

Fig. 7. The effect of re-solution parameter on the bubble concentration for HFIR at 467°C. The He (appm) to dpa ratio is 69 and the helium implantation rate is 6.9×10^{-5} appm/s. (Data from ref. [50].)

are resistant to helium embrittlement. This section describes the results of the present model regarding precipitate effects on helium trapping. Fig. 9 shows the results of such calculations for a simulation of the

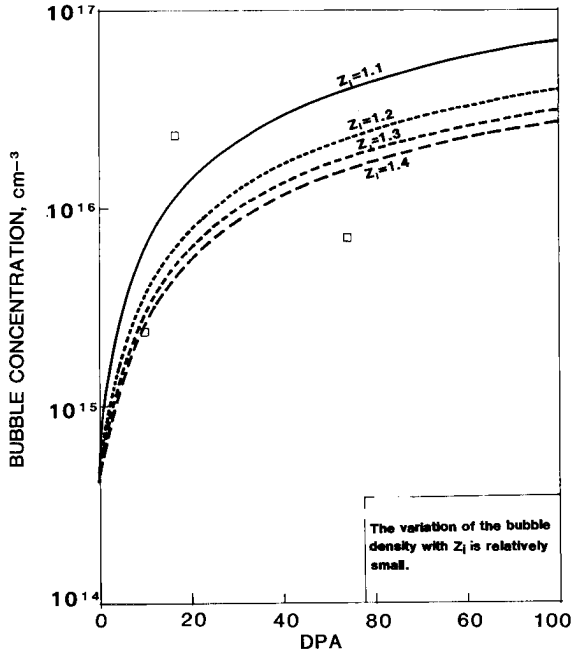

Fig. 8. The dependence of the bubble density on the bias factor as a function of DPA for HFIR condition at 467°C. A re-solution parameter of 10 is used in this case (Data from ref. [50].)

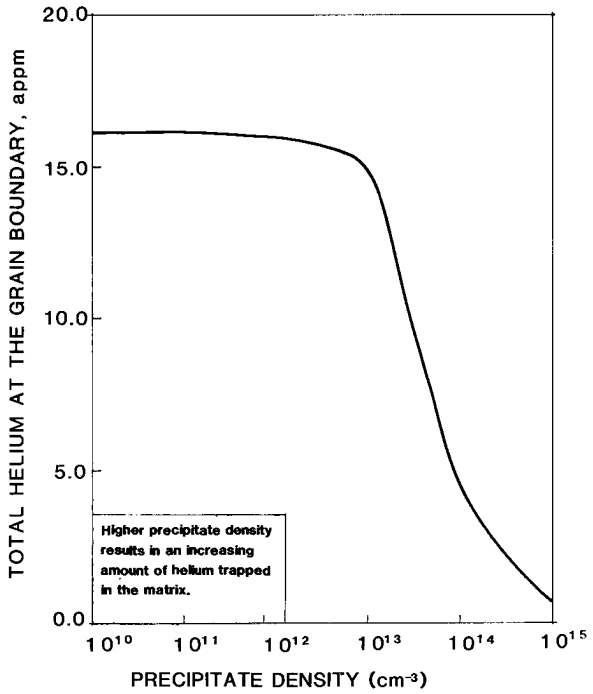

Fig. 9. The effect of matrix precipitates on the amount of helium at the grain boundary. Total injected helium is 150 appm at 625°C.

Argonne experiment. The figure shows the grain boundary gas content (appm), for a total amount of 150 appm injected helium, as a function of the matrix precipitate concentration (cm^{-3}). It is shown that the amount of grain boundary gas is an insensitive function of the matrix precipitate concentration below $\sim 10^{12}$ precipitate/cm^3. The precipitates were assumed here to be spherical, and of an average size $R_p = 100$ Å. The amount of gas finally residing at the grain boundaries decreases sharply as the precipitate density is increased, above 10^{11} cm^{-3}. However, even at relatively moderate densities (10^{14} cm^{-3}), few ppm helium still escape to the grain boundary. Fig. 10 shows helium bubble densities in the matrix, at precipitates, as well as the total density. Homogeneous nucleation of matrix cavities is reduced by the heterogeneous nucleation of cavities at precipitates.

Fig. 11 shows grain boundary helium content (appm) as a function of grain diameter (micrometers), for a total injected helium of 150 appm. The grain boundary gas is a strong function of grain diameter in the range of 10–50 μm. It decreases sharply from about $\frac{1}{3}$ of total injected helium for a grain diameter of 15 μm, to roughly $\frac{1}{30}$ of injected helium for a grain diameter of 15

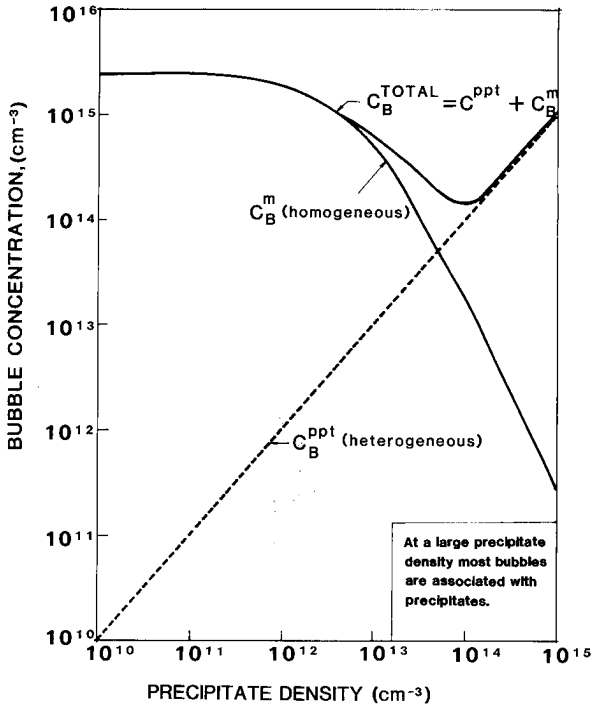

Fig. 10. The effect of precipitates on the bubble concentrations. Total injected helium is 150 appm at 625°C.

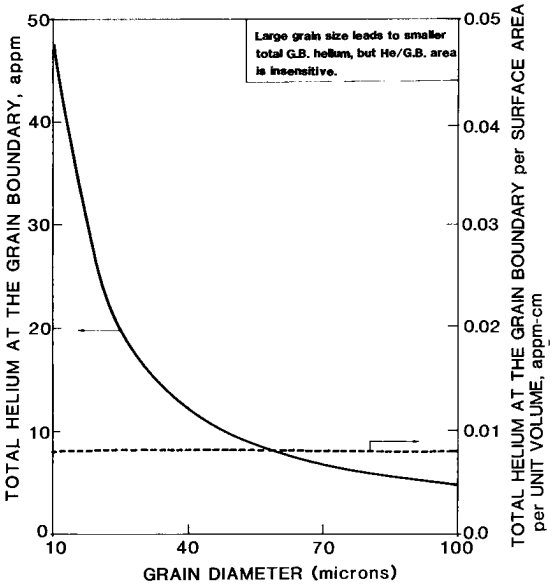

Fig. 11. The influence of grain size on the amount of gas at the grain boundary. Total injected gas is 150 appm at 625°C.

μm, to roughly $\frac{1}{30}$ of injected helium at a diameter of 60 μm, and then saturates thereafter. A moderate grain diameter of 30–60 μm is shown to be sufficient for reducing grain boundary helium trapping. Larger grain sizes do not result in a considerable improvement. The amount of helium per unit surface area is also shown on the same figure. It is shown that this quantity, which determines grain boundary bubble density, is relatively insensitive to grain size. Precipitates have been quantitatively shown to result in a reduction in the amount of helium trapped at grain boundaries. However, for practical precipitate densities few ppm of helium may still reside at grain boundaries. Increasing matrix precipitates is therefore concluded to be more effective in reducing helium embrittlement than increasing grain size.

4. Conclusions

In this study, we have shown reasonable agreement with available data on matrix helium-filled cavity nucleation and growth. This investigation demonstrates the effects of several physical mechanisms that are significant in interpreting experiments and furthering theory development. The following points are concluded:

(1) The injection of helium gas into the solid, either via nuclear reactions or by implantation, cannot be separated from the question of vacancy mobility. It has been shown that large helium concentrations lead to the immobilization of a large fraction of vacancies, leading to a "constrained" mode of cavity growth provided that the cavities or clusters are immobile.

(2) Helium gas re-solution due to the interaction of displacement damage with gas-filled cavities is a process of prime importance to cavity re-nucleation. At high re-solution rates, "dynamic nucleation" is a continuous process throughout irradiation.

(3) Theoretical models, and experiments are both needed to determine the effects of re-solution.

(4) The external source of helium injection can be less important compared to internal helium sources due to gas re-solution effects on gas arrival rates at grain boundaries.

(5) During early irradiation, helium gas is trapped in small vacancy clusters. A large fraction of gas migrates to grain boundaries, until matrix cavity nucleation is complete. When this is achieved, the majority of introduced gas resides in bubbles and a small percentage arrives at grain boundaries. It may

be impossible therefore to completely suppress helium from reaching grain boundaries.

(6) In order for matrix precipitates to act as effective helium traps, their density must be high ($> 10^{13}$–$10^{14}\,cm^{-3}$).

Acknowledgements

Work was partially supported by the US DOE under grant #DE-SG03-84ER52110 with UCLA during Professor Ghoniem's sabbatical leave at KfK. The financial arrangements and consultational help of the radiation damage group at KfK are greatly appreciated.

Nomenclature

a	lattice parameter (cm)
B	Van der Waals' constant (~ 1)
b	re-solution parameter (at./at.)
C_b	matrix bubble concentration (at./at.)
C_g	interstitial helium concentration (at./at.)
C_{gb}	equivalent grain boundary sink concentration (at./at.)
C_{gv}	substitutional helium concentration (at./at.)
C_{2g}	di-interstitial helium cluster concentration (at./at.)
C_{2gv}	concentration of a cluster containing 2-helium atoms and one vacancy (at./at.)
$C_{i,v}$	interstitial/vacancy concentration (at./at.)
C_s^i	equivalent dispersed self-interstitials sink concentration (at./at.)
C_s^v	equivalent dispersed vacancy sink concentration (at./at.)
C_{ppt}	matrix precipitates concentration (at./at.)
C^*	bubble embryo concentration (at./at.)
C_v^e	equilibrium vacancy concentration (at./at.)
d	grain diameter (cm)
$D_{v,i}$	diffusion coefficient of vacancies/interstitials ($cm^2\ s^{-1}$)
e_1	thermal emission probability from a substitutional helium
e_2	thermal emission probability from a vacancy–di-helium cluster
e_3	thermal emission probability from a bubble
e_4	thermal formation probability for a vacancy
e_5	dissociation probability for a di-gas atom cluster
e_3'	thermal emission probability from a precipitate bubble
$E_{g,v}^h$	emission rate constant of a helium atom from a substitutional helium (1/s)
$E_{2g,v}^h$	emission rate constant of a helium from a di-helium single vacancy cluster (1/s)
E_{2g}^h	emission rate constant of a helium from a di-helium cluster (1/s)
E_{vh}^B	binding energy of a substitutional helium (eV)
$E_{v,2h}^B$	binding energy for a vacancy and a di-helium (eV)
E_{2g}^B	binding energy for a di-helium (eV)
$E_{v,b}^B$	binding energy for a vacancy and a bubble (eV)
E_v^f	vacancy formation energy (eV)
f	fraction of vacancies surviving cascade instantaneous recombination
f_{gb}	fraction of total gas at the grain boundary
G	Frenkel pair generation rate (dpa/s)
G_H	helium atom generation rate (at./at./s)
G_{int}^{he}	internal He generation rate (at./at./s)
G_{ext}^{He}	external He generation rate (at./at./s)
J_g	flux of helium to the grain boundary (at./at./s)
K	Boltzmann's Constant (eV/K)
$m_{1,2}$	number of gas atoms in a matrix bubble/precipitate bubble
M_{gb}	total number of gas atoms at the grain boundary
M_{ppt}	total number of gas atoms at precipitates
M_p	matrix precipitate density ($1/cm^3$)
$P_{1,2}$	pressure in a matrix bubble/precipitate bubble (eV/cm^3)
R	radius of a matrix bubble (cm)
R_{pb}	radius of a precipitate bubble (cm)
r_p	radius of a precipitate (cm)
R_p^e	equivalent radius of a bubble–precipitate pair (cm)
$R_{g,v}$	reaction rate between single helium and a vacancy (1/s)
$R_{v,s}$	reaction rate between vacancies and the equivalent vacancy sink (1/s)
$R_{v,2g}$	reaction rate between vacancies and a di-helium cluster (1/s)
$R_{v,gv}$	reaction rate between vacancies and a substitutional helium (1/s)
$R_{v,2gv}$	reaction rate between vacancies and a di-gas single vacancy cluster (1/s)
$R_{v,*}$	reaction rate between vacancies and a critical bubble nucleus (1/s)
$R_{i,2gv}$	reaction rate between interstitials and a di-gas single vacancy cluster (1/s)
$R_{i,*}$	reaction rate between interstitials and a critical bubble nucleus (1/s)
$R_{i,s}$	reaction rate between interstitials and the equivalent interstitial sink (1/s)

$R_{i,gv}$ reaction rate between self interstitials and substitutional helium cluster (1/s)
$R_{g,b}$ reaction rate between interstitial helium and bubbles (1/s)
$R_{g,v}$ reaction rate between interstitial gas atoms and single vacancies (1/s)
$R_{g,g}$ reaction rate between interstitial gas atoms (1/s)
$R_{g,gv}$ reaction rate between interstitial gas atoms and substitutional helium clusters (1/s)
$R_{g,2gv}$ reaction rate between interstitial gas and a di-gas single vacancy cluster (1/s)
$R_{g,gb}$ reaction rate between interstitial gas and the equivalent grain boundary (1/s)
$R_{g,2g}$ reaction rate between interstitial gas and di-gas atom clusters (1/s)
$R_{g,*}$ reaction rate between interstitial gas and a critical bubble nucleus (1/s)
$R_{g,ppt}$ reaction rate between interstitial gas atoms and precipitates (1/s)
t time (s)
T temperature (K)
Z line dislocation bias factor for helium gas
Z_i line dislocation bias factor for self-interstitials
Z_v line dislocation bias factor for vacancies
ρ line dislocation density (cm/cm^3)
Ω atomic volume (cm^3)
γ_b bubble surface tension (eV/cm^2)
α frequency factor for recombination
β frequency factor for helium
γ frequency factor for vacancies
δ re-solution frequency (1/s)
ϵ diffusion-control combinatorial factor for bubbles

References

[1] M.I. Baskes, C.L. Bisson and W.D. Wilson, J. Nucl. Mater. 83 (1979) 139.
[2] G. Carter, D.G. Armour, S.E. Donnelly, D.C. Ingram and R.P. Webb, Harwell Consultants Symposium (October 1979) p. 83.
[3] G. Farrell and W.A. Grant, Radiat. Effects 3 (1970) 249.
[4] R.H.J. Fastenau, A. van Veen, P. Penning and L.M. Caspers, Phys. Status Solidi (A) 47 (1978) 577.
[5] J.E. Inglesfield and J.B. Pendry, Phil. Mag. 34, No. 2 (1976) 205.
[6] D.L. Johnson and J.R Cost, Conf. of the National Bureau of Standards on Defects and Defect Clusters in B.C.C. Metals and their Alloys, Gaithersburg, MD (August 1973) p. 279.
[7] G.R. Odette, P.J. Maziasz and J.A. Spitznagel, J. Nucl. Mater. 103–104 (1981) 1289.
[8] D.B. Poker and J.M. Williams, Appl. Phys. Lett. 40 (1982) 851.
[9] J. Roth, S.T. Picreaux, W. Eckstein, J. Bottiger and R. Behrisch, J. Nucl. Mater. 63 (1976) 120.
[10] W. Schilling, Yamada V Conf. on Point Defects, Tokyo, Japan (October 1981).
[11] F.A. Smidt, Jr. and A.G. Pieper, Conf. of the American Society for Testing and Materials on the Properties of Reactor Structural Alloys After Neutron or Particle Irradiation, ASTM STP 570, Gatlinburg, TN (June 1974), p. 352.
[12] W.D. Wilson and C.L. Bisson, Radiat. Effects 22 (1974) 63.
[13] N.M. Ghoniem, S. Sharafat, J.M. Williams and L.K. Mansur, J. Nucl. Mater. 117 (1983) 96.
[14] H. Böhm, H. Hauk, W. Leo and C. Wassilew, J. Nucl. Mater. 33 (1969) 343.
[15] G.J.C. Carpenter and R.B. Nicholson, Conf. of the International Atomic Energy Agency on the Radiation Damage in Reactor Materials, Vol. II, Vienna (June 1969) p. 383.
[16] K.D. Closs and L. Schäfer, Conf. of the American Society for Testing and Materials on the Effects of Radiation on Substructure and Mechanical Properties of Metals and Alloys, ASTM STP 529, Los Angeles, CA (June 1972) p. 460.
[17] T. Furuta, S. Kawasaki and R. Nagasaki, J. Nucl. Mater. 47 (1973) 65.
[18] K.R. Garr, D. Kramer, C.G. Rhodes and A.G. Pard, J. Nucl. Mater. 28 (1968) 230.
[19] M.Kangilaski, F.T. Zurey, J.J. Perrin and R.A. Wullaert, J. Nucl. Mater. 39 (1971) 117.
[20] R.L. Klueh and J.M. Vitek, J. Nucl. Mater. 117 (1983) 295.
[21] D. Kramer, H.R. Brager, C.G. Rhodes and A.G. Pard, J. Nucl. Mater. 25 (1968) 121.
[22] G.R. Odette, J. Nucl. Mater. 122–123 (1984) 435.
[23] A.A. Sägües, H. Schroeder, W. Kesternich and H. Ullmaier, J. Nucl. Mater. 78 (1978) 289.
[24] H. Shiraishi, N. Nagata and R. Watanabe, J. Nucl. Mater. 87 (1979) 157.
[25] H. Trinkaus, J. Nucl. Mater. 118 (1983) 39.
[26] H. Schroeder, W. Kesternich and H. Ullmaier, Nucl. Engrg. Des./Fusion 2 (1984) 65.
[27] D.R. Harries, A.C. Roberts, G.T. Rogers, J.D.H. Hughes and M. Dewey, Conf. of the International Atomic Energy Agency on the Radiation Damage in Reator Materials, Vol. II, Vienna (June 1969) p. 357.
[28] M.H. Wood and K.L. Kear, J. Nucl. Mater. 118 (1983) 320.
[29] H. Trinkaus and H. Ullmaier, Phil. Mag. A 39, No. 5 (1979) 563.
[30] R. Bullough, D.R. Harries and M.R. Hayns, J. Nucl. Mater. 88 (1980) 312.
[31] L.K. Mansur, W.A. Coghlan and A.D. Brailsford, J. Nucl. Mater. 85–86 (1979) 591.

[32] A.D. Marwick, IBM Report RC9276 (#40786), IBM (1982).
[33] C.P. Chou and N.M. Ghoniem, submitted to J. Nucl. Mater.
[34] N.M. Ghoniem and M.L. Takata, J. Nucl. Mater. 105, Nos. 2–3 (1982) 276.
[35] D. Kaletta, Radiat. Effects 78 (1983) 245.
[36] W. Jäger; R. Manzke, H. Trinkaus, G. Crecelius, R. Zeller, J. Fink and H.L. Bay, J. Nucl. Mater. 111–112 (1982) 674.
[37] R.W. Nelson, J. Nucl. Mater. 31 (1969) 153.
[38] K.C. Russell, Acta Metall. 26 (1978) 1615.
[39] S. Sharafat and N.M. Ghoniem, J. Nucl. Mater. 122, Nos. 1–3 (1984) 531.
[40] H. Trinkaus, Radiat. Effects 78 (1983) 189.
[41] L.K. Mansur, Phil. Mag. A 44 (1981) 867.
[42] J.B. Gibson, A.N. Goland, D.M. Milgram and G.H. Vineyard, Phys. Rev. 120 (1960) 1229.
[43] D.R. Olander, Technical Information Center Publication (1976) p. 208.
[44] R. Fastenau, PhD thesis, Delft University Press (1982) p. 98.
[45] J.R. Matthews and M.H. Wood, Harwell Research Report. TP806 (1979).
[46] J.R. Matthews and M.H. Wood, J. Nucl. Mater. 56 (1980) 439.
[47] A.D. Brailsford and R. Bullough, Phil. Trans. R. Soc. London Ser. A. 302, No. 1465 (1981) 87.
[48] G. Ayrault, H.A. Hoff, F.V. Nolfi, Jr. and A.P.L. Turner, J. Nucl. Mater. 103–104 (1981) 1035.
[49] P. Chou and N.M. Ghoniem, Nucl. Instr. and Meth. B9 (1985) 209.
[50] P. Maziasz and M.L. Grossbeck, J. Nucl. Mater. 103–104 (1981) 987.